

Investigation of Phase-Field models in compressible multiphase flows in a unified high-order and bound-preserving framework

By Z. Huang^{†‡}, S. Mirjalili, M. A. Khanwale, S. S. Jain[¶] AND E. Johnsen[‡]

In the present study, we implement the consistent and conservative Phase-Field method as a unified high-order and bound-preserving framework to investigate different Phase-Field models (the Cahn-Hilliard, conservative Allen-Cahn, and (accurate) conservative diffuse interface models) in compressible multiphase flows. We illustrate that applying shock-capturing schemes for compressible flows introduces nonisotropic numerical diffusion that becomes the dominant effect on the performance of the Phase-Field models, and thus the use of high-order schemes becomes critical. Moreover, we propose and demonstrate two new approaches to improve the interfacial normal calculation for interface compression. Finally, we discuss the different behavior of the Phase-Field models when underresolved interface structures appear.

1. Introduction

Compressible multiphase flows are characterized by interactions between material interfaces and nonlinear waves such as shocks. It is challenging to capture such interactions accurately in numerical simulations as both shocks and interfaces are nonstationary discontinuities from a macroscopic perspective. The diffuse-interface capturing method (Saurel & Pantano, 2018) is widely used for the problem of interest, where, instead of explicitly tracking interfaces, volume fractions of different phases are evolved with the interfaces implied in the transition of the volume fractions. Then, both the shocks and interfaces can be captured with shock-capturing schemes.

One of the long-lasting challenges of the diffuse-interface capturing method is the contradictory role of numerical diffusion. While upwinding (or numerical diffusion) is necessary for capturing shocks, material interfaces continuously diffuse numerically, resulting in numerical mixing of different phases/materials reflected by unbounded growth of interface thickness. To address this issue, recent studies explore the incorporation of Phase-Field models to compete with the numerical diffusion adjacent to material interfaces, resulting in a constant interface thickness (Jain *et al.*, 2020, 2023; Huang & Johnsen, 2023, 2024). The encouraging results in these studies motivate us to further understand the interaction between the shock-capturing schemes and Phase-Field models, as well as the behavior of different Phase-Field models in compressible multiphase flows.

In the present study, we investigate four widely used Phase-Field models and couple them to compressible multiphase flows with the consistent and conservative Phase-Field method (Huang & Johnsen, 2023, 2024). This method is designed for arbitrarily high-order finite-volume and discontinuous Galerkin schemes with guaranteed bound preser-

[†] Department of Mechanical Engineering, University of Alabama

[‡] Department of Mechanical Engineering, University of Michigan

[¶] George W. Woodruff School of Mechanical Engineering, Georgia Institute of Technology

vation, independent of the Phase-Field models selected. The remainder of this study is structured as follows. Section 2 summarizes the computational models and methods. Section 3 illustrates the interaction between shock-capturing schemes and Phase-Field models. Section 4 proposes and demonstrates two new approaches to improve the calculation of interfacial normal for the compression effect. Section 5 further discusses the different behavior of the Phase-Field models in compressible flow problems. Finally, conclusions are drawn in Section 6.

2. Computational models and methods

2.1. Governing equation

We confine the present study to compressible two-phase flows without viscosity and heat conduction to signify the interaction between shock-capturing schemes and Phase-Field models. Such considerations simplify the general equation in Huang & Johnsen, (2023, 2024), leading to

$$\frac{\partial \mathbf{U}}{\partial t} + \nabla \cdot \mathbf{F}^{HB} = \mathbf{S}^{HB} + \nabla \cdot \mathbf{F}^{PF},$$

$$\mathbf{U} = \begin{bmatrix} \alpha_1 \rho_1 \\ \alpha_2 \rho_2 \\ \rho \mathbf{u} \\ \rho E \\ \alpha_1 \end{bmatrix}, \quad \mathbf{F}^{HB} = \begin{bmatrix} \alpha_1 \rho_1 \mathbf{u} \\ \alpha_2 \rho_2 \mathbf{u} \\ \rho \mathbf{u} \otimes \mathbf{u} + P \mathbf{I} \\ (\rho E + P) \mathbf{u} \\ \alpha_1 \mathbf{u} \end{bmatrix}, \quad \mathbf{S}^{HB} = \begin{bmatrix} 0 \\ 0 \\ \mathbf{0} \\ 0 \\ \alpha_1 \nabla \cdot \mathbf{u} \end{bmatrix}, \quad (2.1)$$

$$\mathbf{F}^{PF} = \begin{bmatrix} \mathbf{J}_1 \rho_1 \\ \mathbf{J}_2 \rho_2 \\ \sum_{p=1}^2 \mathbf{J}_p \rho_p \otimes \mathbf{u} \\ \frac{1}{2} \sum_{p=1}^2 \mathbf{J}_p \rho_p \mathbf{u} \cdot \mathbf{u} + \sum_{p=1}^2 \mathbf{J}_p \rho_p e_p \\ \mathbf{J}_1 \end{bmatrix}.$$

Here, the state vector \mathbf{U} contains the mass of each phase ($\alpha_1 \rho_1$ and $\alpha_2 \rho_2$), momentum ($\rho \mathbf{u} = \sum_{p=1}^2 \alpha_p \rho_p \mathbf{u}$), total energy ($\rho E = \frac{1}{2} \rho \mathbf{u} \cdot \mathbf{u} + \sum_{p=1}^2 \alpha_p \rho_p e_p$), and volume fraction of Phase 1 (α_1). The flow velocity is \mathbf{u} , and the pressure is P . The volume fraction of Phase 2 is obtained from $\alpha_2 = 1 - \alpha_1$. The internal energy (e_p) follows the stiffened gas equation of state by Le Métayer *et al.*, (2005) as

$$\rho_p (e_p - D_p) = \frac{1}{\gamma_p - 1} P + \frac{\gamma_p P_p^\infty}{\gamma_p - 1}, \quad 1 \leq p \leq 2, \quad (2.2)$$

where γ_p , P_p^∞ , and D_p are material properties specified in each numerical test.

The Phase-Field flux vector \mathbf{F}^{PF} incorporates the Phase-Field mechanism to compressible multiphase flows in a consistent and conservative manner, satisfying the conservation of mass, momentum, and energy; second law of thermodynamics; and Galilean invariance. Therefore, Eq. (2.1) allows different Phase-Field models (represented by \mathbf{J}_1 and $\mathbf{J}_2 = -\mathbf{J}_1$) to be implemented. For convenience, we use $\alpha = \alpha_1$ and $\mathbf{J} = \mathbf{J}_1$ when there is no ambiguity.

2.2. Numerical approach

Eq. (2.1) is solved from a finite-volume procedure detailed in Huang & Johnsen, (2023, 2024). The hyperbolic step is first performed as

$$\frac{\partial \bar{\mathbf{U}}}{\partial t} + \nabla \cdot \hat{\mathbf{F}}^{HB}(\mathbf{U}^L, \mathbf{U}^R) = \hat{\mathbf{S}}^{HB}(\bar{\mathbf{U}}, \mathbf{U}^L, \mathbf{U}^R), \quad (2.3)$$

where $\bar{\mathbf{U}}$ is the cell-averaged value and $\mathbf{U}^{L,R}$ are the reconstructed values at cell faces. The HLL approximate Riemann solver (Toro, 2009) is used in the present study, represented by $\hat{\mathbf{F}}^{HB}$ and $\hat{\mathbf{S}}^{HB}$. The time step is determined from the Courant-Friedrichs-Lewy (CFL) condition: $\Delta t(\max_x |\mathbf{u}| + c)/\Delta x = \text{CFL}$, where c is the sound speed.

Then, the Phase-Field step is performed with the reduction-consistent formulation as

$$\frac{\partial \bar{\mathbf{U}}}{\partial \tau} = \nabla \cdot \hat{\mathbf{F}}^{PF}(\mathbf{U}^L, \mathbf{U}^R; \nabla Q), \quad (2.4)$$

from $\tau = 0$ to $\tau = \Delta t$. Here, Q (or ∇Q) is an auxiliary variable extracting the information of Phase-Field models (represented by \mathbf{J} or $\nabla \cdot \mathbf{J}$) via

$$\nabla \cdot (\alpha(1 - \alpha)\nabla Q) = \nabla \cdot \mathbf{J}, \quad (2.5)$$

due to the consistency of reduction (Huang *et al.*, 2020, 2021, 2022). Once ∇Q is available, $\hat{\mathbf{F}}^{PF}(\mathbf{U}^L, \mathbf{U}^R; \nabla Q)$ is computed with the upwind and downwind values of \mathbf{U} at cell faces based on the direction of ∇Q . The CFL condition in the Phase-Field step is $\Delta \tau \max_x |\nabla Q|/\Delta x = \text{CFL}^{PF}$.

In the present study, both Eq. (2.3) and Eq. (2.4) are evolved with the third-order total variation diminishing (TVD) Runge-Kutta time stepping (Gottlieb & Shu, 1998). As analyzed in Huang & Johnsen, (2023, 2024), an arbitrarily high-order polynomial reconstruction can be implemented without violating the volume fraction boundedness or mass positivity when appropriate CFL and CFL^{PF} are used, leading to a high-order and bound-preserving finite-volume scheme for compressible multiphase flows with different Phase-Field models. Interested readers should refer to Huang & Johnsen, (2023, 2024) for details.

2.3. Phase-Field models

In the present study, we consider four different Phase-Field models that share an identical equilibrium interfacial profile in one dimension, expressed as

$$\alpha = \mathcal{F}(\psi) = \frac{1}{2} \left(1 + \tanh \left(\frac{\psi}{\sqrt{2}\eta} \right) \right), \quad (2.6)$$

where ψ denotes the signed distance to interfaces ($\psi = x - x_I$ in one dimension with x_I the location of the interface), and η controls the interface thickness. We further define $\mathcal{G}(\phi) = \mathcal{F}^{-1}(\phi)$, as the inverse function of $\mathcal{F}(\cdot)$.

The Cahn-Hilliard model (CH) (Cahn & Hilliard, 1958) with degenerate mobility (Khanwale *et al.*, 2022) is

$$\nabla \cdot \mathbf{J} = \nabla \cdot (M\alpha(1 - \alpha)\nabla \xi), \quad \xi = \frac{1}{\eta^2} \frac{dg}{d\alpha} - \nabla^2 \alpha, \quad g(\alpha) = \alpha^2(1 - \alpha)^2, \quad (2.7)$$

where M is the magnitude of the mobility, ξ the chemical potential, and $g(\alpha)$ the Ginzburg-Landau double-well potential.

The conservative Allen-Cahn model (CAC) (Brassel & Bretin, 2011) is

$$\nabla \cdot \mathbf{J} = -M\xi + \sqrt{g(\alpha)} \frac{\int_{\Omega} M\xi d\Omega}{\int_{\Omega} \sqrt{g(\alpha)} d\Omega}, \quad (2.8)$$

where ξ and $g(\alpha)$ are the same as those in Eq. (2.7). This model has been implemented in compressible multiphase flows (Huang & Johnsen, 2023).

The Conservative Diffuse Interface model (CDI) (Chiu & Lin, 2011; Mirjalili *et al.*, 2020) is

$$\nabla \cdot \mathbf{J} = \nabla \cdot \left(M \left(\nabla \alpha - \frac{\sqrt{2}}{\eta} \alpha(1-\alpha) \mathbf{n} \right) \right), \quad (2.9)$$

where $\mathbf{n} = \nabla \alpha / |\nabla \alpha|$ is the interfacial normal. This model has been implemented in compressible multiphase flows (Jain *et al.*, 2020, 2023).

The Accurate Conservative Diffuse Interface model (ACDI) (Jain, 2022) is

$$\nabla \cdot \mathbf{J} = \nabla \cdot \left(M \left(\nabla \alpha - \frac{1}{2\sqrt{2}\eta} \operatorname{sech}^2 \left(\frac{\psi}{\sqrt{2}\eta} \right) \mathbf{n} \right) \right), \quad (2.10)$$

where $\psi = \mathcal{G}(\alpha)$ and $\mathbf{n} = \nabla \psi / |\nabla \psi|$.

For CAC, which is not a flux-based model, a linear system resulting from discretizing Eq. (2.5) has to be solved for Q , after which ∇Q is computed (Huang & Johnsen, 2023, 2024). On the other hand, CH, CDI, and ACDI are flux-based, and $\nabla Q = \mathbf{J} / (\alpha(1-\alpha))$ is directly obtained from Eq. (2.5). For CH in Eq. (2.7), it is straightforward to obtain $\nabla Q = M\nabla \xi$. We note that ∇Q can be explicitly written as $\nabla Q = \frac{\sqrt{2}M}{\eta} (\nabla \psi - \mathbf{n})$ for CDI and ACDI, after using $\psi = \mathcal{G}(\alpha)$. However, our primary tests did not show significant differences when $\nabla Q = \frac{\sqrt{2}M}{\eta} (\nabla \psi - \mathbf{n})$ is used. The present study applies $M = 3\eta^3 \max |\mathbf{u}|$ for CH and $M = 0.5\eta \max |\mathbf{u}|$ for the others. The Phase-Field models as well as Eq. (2.5) are computed with the second-order central difference, linear interpolation, and mid-point rule wherever they apply.

3. Interaction between shock-capturing schemes and Phase-Field models

To illustrate the interaction between the shock-capturing schemes and Phase-Field models, we design the relaxation problem as

$$\partial_t \mathbf{U} + \nabla \cdot \mathbf{F}^{HB} = \mathbf{S}^{HB}, \quad 0 < t < 10; \quad \partial_t \mathbf{U} = \nabla \cdot \mathbf{F}^{PF}, \quad t \geq 10; \quad (3.1)$$

with an initial condition $(\rho_1, \gamma_1, P_1^\infty, \rho_2, \gamma_2, P_2^\infty, u, v, P) = (1, 1.4, 0, 2, 1.6, 0.1, 0, 0, 1)$ and α from Eq. (2.6) where $\psi = 0.5 - \sqrt{x^2 + y^2}$. The doubly periodic domain is $[-1, 1] \times [-1, 1]$, discretized by 128×128 grid cells. Before $t = 10$, the Phase-Field flux vector is not activated. As a result, the circle with a radius of 0.5 in the middle of the domain is smeared by the numerical diffusion from the shock-capturing schemes. After $t = 10$, only the Phase-Field flux vector is activated to correct the distorted interfacial profile.

We use both the MUSCL and fifth-order WENO reconstructions with $\eta = \Delta x$. In all the problems investigated in the present study, $\text{CFL} = \text{CFL}^{PF} = 0.3$ is always used except when the CH model is implemented. In that case, $\text{CFL} = 0.01$ due to a fully explicit calculation of CH that is a fourth-order partial differential equation (PDE).

Figure 1 shows the volume fraction α at $t = 0$, $t = 10$, and $t = 20$ with MUSCL reconstruction. The interface is difficult to identify at $t = 10$ because of the strong

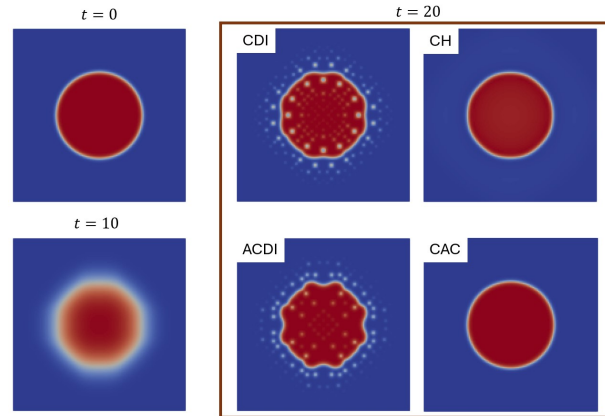


FIGURE 1. Volume fraction α at $t = 0$, $t = 10$, and $t = 20$ in the relaxation problem with the MUSCL reconstruction from different Phase-Field models.

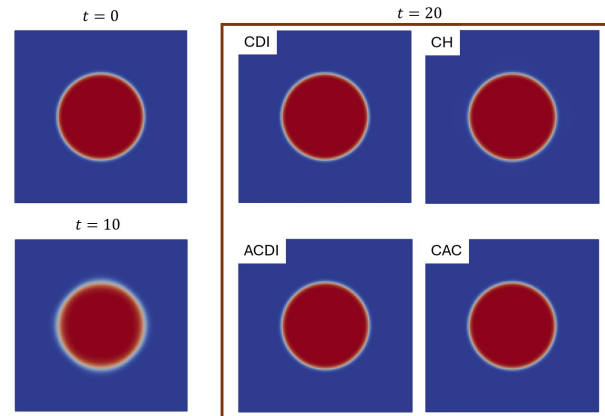


FIGURE 2. Volume fraction α at $t = 0$, $t = 10$, and $t = 20$ in the relaxation problem with the fifth-order WENO reconstruction from different Phase-Field models.

smearing from the numerical diffusion. Moreover, due to the dimension-by-dimension nature of the shock-capturing schemes, the interface is thickened more significantly along the coordinate axes, implying that the numerical diffusion is nonisotropic. Neither CDI nor ACDI is able to recover the initial circular interface because the interfacial normal can no longer be accurately calculated given a highly distorted interface profile. However, both CH and CAC recover the circular shape because these two models drive the phase field toward minimizing the free energy.

Figure 2 shows the corresponding results with the fifth-order WENO reconstruction. The implementation of a high-order reconstruction significantly reduces the numerical diffusion, resulting in a sharper and less distorted interface at $t = 10$, while the nonisotropic effect is still observable. Given such a less distorted interface, all the Phase-Field models successfully recover the initial circular interface after their activation.

CDI is sensitive to the calculation of its compression term $\alpha(1 - \alpha)\mathbf{n}$ at cell faces. To address this, we compared the results from three calculation methods of the compression term (see Figure 3). By default (labeled as CDI), we first evaluate the interfacial normal at cell centers with the second-order central difference and then linearly interpolate α and

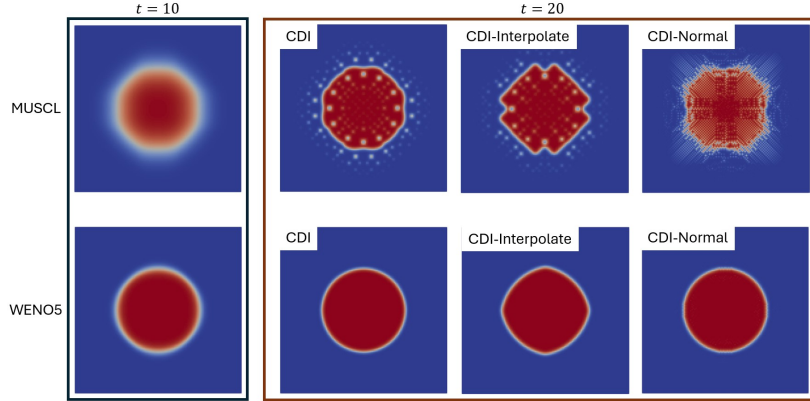


FIGURE 3. Volume fraction α at $t = 10$ and $t = 20$ in the relaxation problem with different compression calculations for CDI.

\mathbf{n} to cell faces individually (Jain *et al.*, 2023). Another way (labeled as CDI-Interpolate) is to first calculate the entire compression term at cell centers and then perform the linear interpolation. A third option (labeled as CDI-Normal) is to directly evaluate the interfacial normal at cell faces with a compact stencil (Desjardins *et al.*, 2008). As shown in Figure 3, the default calculation provides the most satisfactory result. CDI-Interpolate tends to produce sharp corners, while CDI-Normal tends to produce spurious oscillations.

4. New approaches for interfacial normal calculation

As observed in the relaxation problem in Section 3, the nonisotropic numerical diffusion introduced by shock-capturing schemes distorts the interface profile represented by α or $\psi = \mathcal{G}(\alpha)$, leading to an inaccurate interfacial normal in CDI and ACDI. As a result, the compression effect is pointed in a wrong direction. Although using a higher-order reconstruction can alleviate the issue, we here propose two approaches that use an alternative quantity to improve the interfacial normal calculation for CDI and ACDI. We note that the two new approaches are implemented right after the hyperbolic step.

The first approach calculates the interfacial normal from $\mathbf{n} = \nabla \tilde{H} / |\nabla \tilde{H}|$, where \tilde{H} is a smoothed Heaviside function from the diffusion equation as

$$\frac{\partial \tilde{H}}{\partial s} = D \nabla^2 \tilde{H}, \quad s > 0; \quad \tilde{H} = \text{Heaviside}(\alpha - 0.5), \quad s = 0. \quad (4.1)$$

The idea of this diffusion approach is to develop an isotropic diffused profile adjacent to the interface, removing the nonisotropic effect from the shock-capturing schemes.

The second approach calculates the interfacial normal from $\mathbf{n} = \nabla \tilde{\psi} / |\nabla \tilde{\psi}|$, where $\tilde{\psi}$ is a signed-distance function from the reinitialization equation (Sussman *et al.*, 1994) as

$$\frac{\partial \tilde{\psi}}{\partial s} = \text{sign}(\mathcal{G}(\alpha)) (1 - |\nabla \tilde{\psi}|), \quad s > 0; \quad \tilde{\psi} = \mathcal{G}(\alpha), \quad s = 0. \quad (4.2)$$

The idea of this reinitialization approach is to obtain a signed-distance function that is smooth adjacent to the interface, as in Desjardins *et al.*, (2008).

Figure 4 compares the two new approaches (labeled as CDI-Diffusion and CDI-Reinitial) to the original approach (labeled as CDI) in the relaxation problem in Section 3. Both of

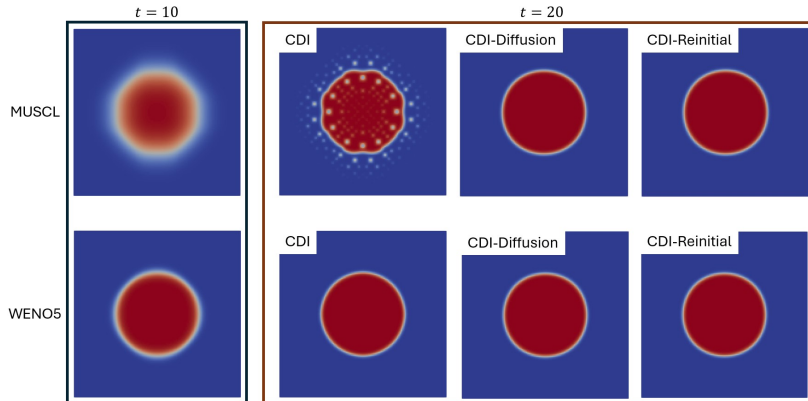


FIGURE 4. Volume fraction α at $t = 10$ and $t = 20$ in the relaxation problem with different interfacial normal calculations for CDI.

the new approaches successfully recover the initial circular interface no matter whether the MUSCL or fifth-order WENO reconstruction is used. We observe the same improvement when using ACDI (not shown). These results suggest that the nonisotropic effect is the dominant source of error for CDI and ACDI. These two new approaches are further tested in Section 5 in flow problems with underresolved interface structures.

5. Multiphase flow problems

5.1. Long-time advection

We consider an advection of a circular bubble over a long period of time. The problem setup is the same as the relaxation problem in Section 3 except that $u = v = 1$ at $t = 0$. Therefore, the circular bubble is translated diagonally.

Figure 5 shows the volume fraction α at $t = 0$ and $t = 10$ with the MUSCL reconstruction. At $t = 10$, five periods of advection are completed, and the bubble returns to the center of the domain. All of the Phase-Field models maintain a uniform interface thickness effectively, compared to the one without Phase-Field models. It is not surprising that both CDI and ACDI introduce obvious interface deformation due to the inaccurate interfacial normal calculation directly from α (CDI) or $\mathcal{G}(\alpha)$ (ACDI) that is significantly distorted by nonisotropic numerical diffusion. The improvement from the two new approaches (CDI-Diffusion and CDI-Reinitial) is obvious. Although both CH and CAC drive the phase field toward minimizing the free energy, CAC is less sensitive to perturbations from numerical diffusion and maintains the circular shape much better.

Figure 6 shows the corresponding results with the fifth-order WENO reconstruction, and all the Phase-Field models benefit from the higher-order reconstruction. The bubble shape at $t = 10$ from CDI, ACDI, and CH is less deformed, although corners along the coordinate axes are still formed. For CDI-Diffusion, CDI-Reinitial, and CAC, the final bubble shape is indistinguishable from the initial condition. Comparing Figure 6 with Figure 5, we observe that CDI-Diffusion and CDI-Reinitial with MUSCL are even more accurate than CDI and ACDI with the fifth-order WENO reconstruction.

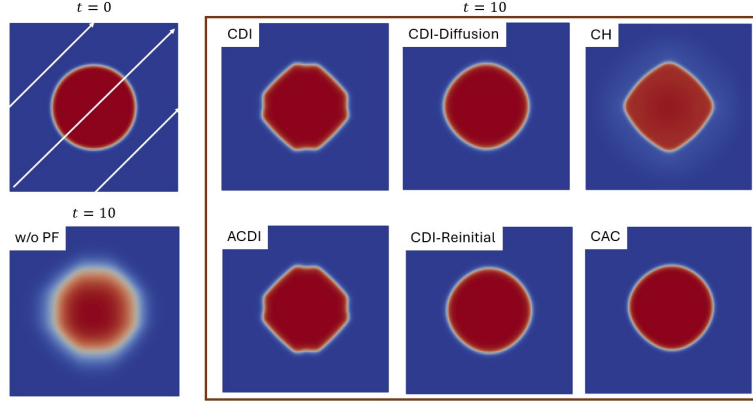


FIGURE 5. Volume fraction α at $t = 0$ and $t = 10$ in the long-time advection problem with the MUSCL reconstruction from different Phase-Field models.

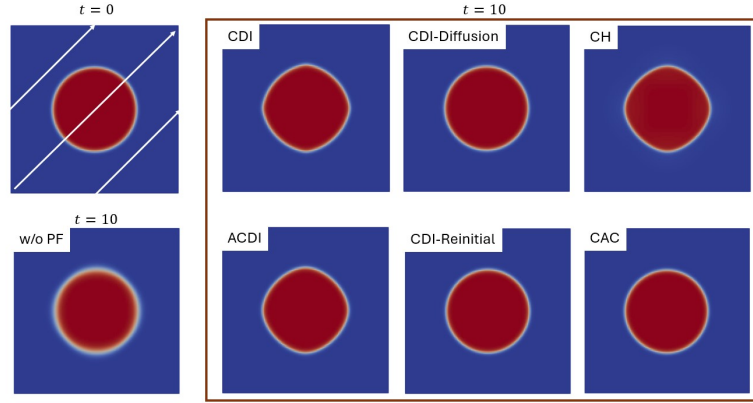


FIGURE 6. Volume fraction α at $t = 0$ and $t = 10$ in the long-time advection problem with the fifth-order WENO reconstruction from different Phase-Field models.

5.2. Shock-bubble interaction

We further investigate the behavior of different Phase-Field models in the shock-bubble interaction problem (Haas & Sturtevant, 1987): A Mach 1.22 shock traveling in the air impinges on a helium cylindrical bubble. The computational domain is $[-1.5, 4.8] \times [0, 1.5]$, covering only the upper half of the problem due to symmetry. The left and right boundaries are the outflow, and the top is the slip wall. The shock is initially at $x = -0.85$, and the bubble with a radius of 0.8 is at $x = y = 0$. The domain is discretized by 512×128 grid cells, and the fifth-order WENO reconstruction is used.

Figure 7 shows the density ρ of different Phase-Field models at selected moments. All the Phase-Field models effectively prevent the interface thickening introduced by the numerical diffusion from shock-capturing schemes. Moreover, the wave structure away from the interface is identical with different Phase-Field models, verifying that the Phase-Field effect is localized adjacent to interfaces.

The difference among the Phase-Field models is subtle at the beginning (before $t = 0.012$) when all the interface structures are well resolved by the grid, although one can still observe a slightly less smooth interface by CDI and ACDI. The major difference appears when the interface rolls up ($t = 0.018$). CDI and ACDI break the interface and form four

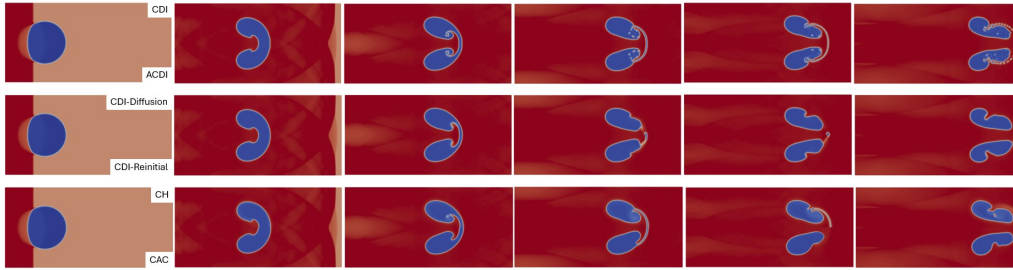


FIGURE 7. Density ρ at (from left to right) $t = 0.001, 0.012, 0.018, 0.022, 0.025,$ and 0.030 in the shock-bubble interaction problem with the fifth-order WENO reconstruction from different Phase-Field models. The helium bubble is in blue.

tiny bubbles, while only a single small bubble is formed when applying CH. This small interface structure is kept by CDI and ACDI, while it is dissolved to the bulk phase from CH. There is no breakup using CDI-Diffusion, CDI-Reinitial, and CAC, but the interface appears more diffusive near the roll up with CDI-Diffusion and CDI-Reinitial. This is because both the diffusion Eq. (4.1) and reinitialization Eq. (4.2) tend to smooth out the interface structures underresolved by the grid. Another difference is observed after the filament is formed ($t \geq 0.022$). As the filament gets thinner, it breaks into several tiny bubbles when applying CDI and ACDI. The filament in CDI-Diffusion and CDI-Reinitial disappears earliest, consistent with the behavior of Eq. (4.1) and Eq. (4.2), and instead forms a small bubble on the middle line. This small bubble is maintained in CDI-Diffusion but finally disappears in CDI-Reinitial. The filament in CAC stays for a longer period of time than that in CDI-Diffusion and CDI-Reinitial but completely disappears instantly. The filament in CH disappears very slowly, and a small air bubble is formed and maintained inside the helium bubble (in blue) at the end.

Instead of concluding which Phase-Field model is superior, we aim to illustrate the intrinsic behavior of different Phase-Field models, enabling scientific understanding of their simulation results in other compressible multiphase flows.

6. Conclusions

Under a unified high-order and bound-preserving framework provided by the consistent and conservative Phase-Field method (Huang & Johnsen, 2023, 2024), we investigated the behavior of the CH, CAC, CDI, and ACDI Phase-Field models in compressible multiphase flows. We first illustrated the interaction between the shock-capturing schemes and the Phase-Field models. When coupling the Phase-Field models with compressible multiphase flows solved by shock-capturing schemes, the nonisotropic numerical diffusion from shock-capturing schemes is most influential to the performance of the Phase-Field models. For CDI and ACDI in particular, the nonisotropic numerical diffusion distorts the interface profile, which then produces an interfacial normal that generates compression in a wrong direction, resulting in spurious interface deformation. In addition to increasing the order of accuracy of discretization, which reduces the amount of numerical diffusion, we proposed the diffusion and reinitialization approaches for interfacial normal calculation in CDI and ACDI, and demonstrated their improvement for well-resolved interface structures. Both CDI and ACDI tend to break an underresolved interface structure into small pieces and then maintain them, while CH tends to break the interface structure into a piece bigger than those from CDI/ACDI and then dissolves it gradually to the bulk

phase. It is possible that CDI-Diffusion and CDI-Reinitial break the interface structure that is small but still resolved by the grid and then turn it into a larger structure. The CAC model has the least tendency to break the interface or to maintain underresolved interface structures.

We finally note that the CH model is a fourth-order PDE, and its current fully explicit implementation requires a CFL number more than 10 times smaller than the other Phase-Field models that are second-order PDEs. Therefore, quantifying efficiency is one of the future works. Furthermore, to better resolve interfaces, adaptive mesh refinement is an attractive technique to implement.

REFERENCES

- BRASSEL, M. & BRETIN, E. 2011 A modified phase field approximation for mean curvature flow with conservation of the volume. *Math. Methods Appl. Sci.* **10**, 1157–1180.
- CAHN, J. & HILLIARD, J. 1958 Free energy of a nonuniform system: I. interfacial free energy. *J. Chem. Phys.* **28**, 258–267.
- CHIU, P. H. & LIN, Y. T. 2011 A conservative phase field method for solving incompressible two-phase flows. *J. Comput. Phys.* **230**, 185–204.
- DESJARDINS, O., MOUREAU, V. & PITSCH, H. 2008 An accurate conservative level set/ghost fluid method for simulating turbulent atomization. *J. Comput. Phys.* **227**, 8395–8416.
- GOTTLIEB, S. & SHU, C.-W. 1998 Total variation diminishing Runge-Kutta schemes. *Math. Comput.* **67**, 73–85.
- HUANG, Z., LIN, G. & ARDEKANI, A. M. 2020 Consistent and conservative scheme for incompressible two-phase flows using the conservative Allen-Cahn model. *J. Comput. Phys.* **420**, 109718.
- HUANG, Z., LIN, G. & ARDEKANI, A. M. 2021 A consistent and conservative volume distribution algorithm and its applications to multiphase flows using Phase-Field models. *Int. J. Multiphas. Flow.* **142**, 103727.
- HUANG, Z., LIN, G. & ARDEKANI, A. M. 2022 Implementing contact angle boundary conditions for second-order Phase-Field models of wall-bounded multiphase flows. *J. Comput. Phys.* **471**, 111619.
- HUANG, Z. & JOHNSEN, E. 2023 A consistent and conservative Phase-Field method for compressible multiphase flows with shocks. *J. Comput. Phys.* **488**, 112195.
- HUANG, Z. & JOHNSEN, E. 2024 A consistent and conservative Phase-Field method for compressible N -phase flows: consistent limiter and multiphase reduction-consistent formulation. *J. Comput. Phys.* **501**, 112801.
- HAAS, J.-F. & STURTEVANT, B. 1987 Interaction of weak shock waves with cylindrical and spherical gas inhomogeneities. *J. Fluid Mech.* **181**, 41–76.
- JAIN, S. S., MANI, A. & MOIN, P. 2020 A conservative diffuse-interface method for compressible two-phase flows. *J. Comput. Phys.* **418**, 109606.
- JAIN, S. S. 2022 Accurate conservative phase-field method for simulation of two-phase flows. *J. Comput. Phys.* **469**, 111529.
- JAIN, S. S., ADLER, M., WEST, J., MANI, A., MOIN, P. & LELE, S. 2023 Assessment of diffuse-interface methods for compressible multiphase fluid flows and elastic-plastic deformation in solids. *J. Comput. Phys.* **475**, 111866.

- KHANWALE, M. A., SAURABH, K., ISHII, M., SUNDAR, H. & GANAPATHYSUBRAMANIAN, B. 2022 Breakup dynamics in primary jet atomization using mesh-and interface-refined Cahn-Hilliard Navier-Stokes. *arXiv Preprint* arXiv:2209.13142.
- LE MÉTAYER, O., MASSONI, J. & SAUREL, R. 2005 Modelling evaporation fronts with reactive Riemann solvers. *J. Comput. Phys.* **205**, 567–610.
- MIRJALILI, S., IVEY, C. B. & MANI, A. 2020 A conservative diffuse interface method for two-phase flows with provable boundedness properties. *J. Comput. Phys.* **401**, 109006.
- SAUREL, R. & PANTANO, C. 2018 Diffuse-interface capturing methods for compressible two-phase flows. *Annu. Rev. Fluid Mech.* **50**, 105–130.
- SUSSMAN, M., SMEREKA, P. & OSHER, S. 1994 A level set approach for computing solutions to incompressible two-phase flow. *J. Comput. Phys.* **114**, 146–159.
- TORO, E. 2009 *Riemann Solvers and Numerical Methods for Fluid Dynamics*. Springer-Verlag.